Reprinted from LANGMUIR, 1994, 10.

Combining Micromachining and Molecular Self-Assembly To Fabricate Microelectrodes

Nicholas L. Abbott*

Department of Chemical Engineering and Materials Science, University of California, Davis, California 95616

Debra R. Rolison*

Code 6170, Surface Chemistry Branch, Naval Research Laboratory, Washington, D.C. 20375-5342

George M. Whitesides*

Department of Chemistry, Harvard University, Cambridge, Massachusetts 02138

Received February 16, 1994. In Final Form: May 9, 1994[⊗]

This paper describes three types of gold electrodes, each with at least one spatial dimension as small as 1 μm, fabricated using combinations of micromachining and molecular self-assembly. (i) Large-area (>0.1 mm^2) arrays of band-type electrodes were formed by machining micrometer-wide grooves of bare gold into gold film covered with a ~23-Å-thick, electrically insulating, self-assembled monolayer (SAM) of $CH_3(CH_2)_{15}S$. (ii) Micrometer-wide, centimeter-long, 100-nm-thick gold electrodes supported on glass were fabricated by patterning a gold film with monolayers of $CH_3(CH_2)_{15}S$ and $HO(CH_2)_2S$, and selectively etching the regions of gold covered with $HO(CH_2)_2S$ using an aqueous solution of CN^- saturated with O_2. (iii) Two microelectrodes, each with electrochemically active areas as small as 100 nm × 1 μm and separated from each other by a distance of 1 μm, were formed by machining a 1-μm-wide gap into a supported gold wire covered with an electrically insulating SAM of $CH_3(CH_2)_{15}S$; exposed gold on either side of the machined gap formed the electrochemically active surfaces of the microelectrode pair.

Introduction

Microelectrodes are electrodes with at least one micrometer-scale dimension.[1,2] These small electrodes can be used to investigate electrochemistry with a spatial resolution on the order of the size of the electrode. Because microelectrodes have small capacitances (due to their small area) and because the flux of redox-active species to small electrodes is high (due to nonplanar diffusion), these electrodes can also be used to make electrochemical measurements on fast processes.[3] These characteristics, and others, have lead to applications of microelectrodes in electrophysiology,[4] the measurement of kinetics of heterogeneous chemical reactions,[2,5] and fabrication of electroanalytical devices.[6] Only one dimension of an electrode needs to be small for fast response times (<milliseconds). Arrays of band-type microelectrodes—electrodes with micrometer-scale lateral dimensions and millimeter-scale longitudinal dimensions—combine relatively large electrode areas (>1000 μm^2) with millisecond response times.[7] Electrodes with both lateral and longitudinal dimensions in the micrometer range can measure, in principle, the presence of redox-active analytes in volumes as small as ~1 fL (1 μm^3).

Self-assembled monolayers (SAMs) of long-chain alkanethiolates on gold have been used extensively to design and synthesize organic surfaces with well-defined chemical and physical properties.[8-23] In this work we used SAMs for two reasons. First, SAMs[24] of $CH_3(CH_2)_{15}S$

[⊗] Abstract published in *Advance ACS Abstracts,* June 15, 1994.

(1) Microelectrodes can also be defined by their cyclic voltammograms: microelectrodes are those electrodes for which mass transport is rapid, and therefore, little or no hysteresis is present in their cyclic voltammograms. For reviews on microelectrodes see: *Microelectrodes: Theory and Applications*; Montenegro, M. I., Queiros, M. A., Daschbach, J. L., Eds.; Kluwer Academic: Boston, 1991. Wightman, R. M.; Wipf, D. O. In *Electroanalytical Chemistry: A Series of Advances*; Bard, A. J., Ed.; Marcel Dekker: New York, 1989; Vol. 15, pp 267.

(2) Fleischmann, M.; Pons, S.; Rolison, D. R.; Schmidt, P. P. *Ultramicroelectrodes*; Datatech Systems: Morgantown, NC, 1987; see also references cited therein.

(3) Howell, J. O.; Wightman, R. M. *Anal. Chem.* **1991**, *63*, 24. Wightman, R. M.; Wipf, D. O. *Acc. Chem. Res.* **1990**, *23*, 64.

(4) *Electrophysiology: A Practical Approach*; Wallis, D. I., Ed.; Oxford University Press: Oxford, 1993. *Glass Microelectrodes*; Lavallee, M., Schanne, O. F., Hebert, N. C., Eds.; Wiley: New York, 1969.

(5) Baranski, A. S.; Winkler, K.; Fawcett, W. R. *J. Electroanal. Chem.* **1991**, *313*, 367.

(6) Ammann, D. *Ion-Selective Microelectrodes: Principles, Design, and Application*; Springer-Verlag: Berlin, New York, 1986.

(7) Wehmeyer, K. R.; Deakin, M. R.; Wightman, R. M. *Anal. Chem.* **1985**, *57*, 1913. Thormann, W.; van den Bosch, P.; Bond, A. M. *Anal. Chem.* **1985**, *57*, 2764. White, H. S. *J. Electroanal. Chem.* **1989**, *264*, 281.

(8) Kumar, A.; Biebuyck, H. A.; Abbott, N. L.; Whitesides, G. M. *J. Am. Chem. Soc.* **1992**, *114*, 9188. Abbott, N. L.; Kumar, A.; Whitesides, G. M. *Chem. Mater.* **1994**, *6*, 596.

(9) Abbott, N. L.; Folkers, J. P.; Whitesides, G. M. *Science (Washington, D.C.)* **1992**, *257*, 1380.

(10) *Formation*: Nuzzo, R. G.; Allara, D. L. *J. Am. Chem. Soc.* **1983**, *105*, 4481. Nuzzo, R. G.; Fusco, F. A.; Allara, D. L. *J. Am. Chem. Soc.* **1987**, *109*, 2358. Bain, C. D.; Troughton, E. B.; Tao, Y.-T.; Evall, J.; Whitesides, G. M.; Nuzzo, R. G. *J. Am. Chem. Soc.* **1989**, *111*, 321. Whitesides, G. M.; Laibinis, P. E. *Langmuir* **1990**, *6*, 87 and references cited within.

(11) *Wetting*: Bain, C. D.; Whitesides, G. M. *J. Am. Chem. Soc.* **1988**, *110*, 5897. Bain, C. D.; Whitesides, G. M. *Langmuir* **1989**, *5*, 1370. Dubois, L. H.; Zegarski, B. R.; Nuzzo, R. G. *J. Am. Chem. Soc.* **1990**, *112*, 570. Laibinis, P. E.; Whitesides, G. M. *J. Am. Chem. Soc.* **1992**, *114*, 1990. Abbott, N. L.; Whitesides, G. M.; Racz, L. M.; Szekely, J. *J. Am. Chem. Soc.* **1994**, *116*, 290. Abbott, N. L.; Whitesides, G. M. *Langmuir* **1994**, *10*, 1493.

(12) *Adhesion*: Allara, D. L.; Hebard, A. F.; Padden, F. J.; Nuzzo, R. G.; Falcone, D. R. *J. Vac. Sci. Technol., A* **1983**, 376. Stewart, K. R.; Whitesides, G. M.; Godfried, H. P.; Silvera, I. F. *Rev. Sci. Instrum.* **1986**, *57*, 1381. Czanderna, A. W.; King, D. E.; Spaulding, D. *J. Vac. Sci. Technol., A* **1991**, *9*, 2607. Armstrong, F. A.; Hill, H. A. O.; Walton, N. J. *Acc. Chem. Res.* **1988**, *21*, 407. Pale-Grosemange, C.; Simon, E. S.; Prime, K. L.; Whitesides, G. M. *J. Am. Chem. Soc.* **1991**, *113*, 12. Haussling, L.; Michel, B.; Ringsdorf, H.; Rohrer, H. *Angew. Chem., Int. Ed. Engl.* **1991**, *30*, 569. Tarlov, M. J.; Bowden, E. F. *J. Am. Chem. Soc.* **1991**, *113*, 1847. Prime, K. L.; Whitesides, G. M. *Science (Washington, D.C.)* **1991**, *252*, 1164. Haussling, L.; Ringsdorf, H.; Schmitt, F.-J.; Knoll, W. *Langmuir* **1991**, *7*, 1837.

0743-7463/94/2410-2672$04.50/0

effectively block the transfer of electrons between a film of gold and a contacting aqueous solution of redox-active molecules.[14-23] Regions of bare[25] gold micromachined[26] into these surfaces behave as microelectrodes.[27] Second, SAMs of $CH_3(CH_2)_{15}S$ protect films of gold from wet chemical etching by solutions of CN^- saturated with O_2:[8] SAMs of $HO(CH_2)_2S$ do not, however, form a protective barrier to this etchant. Selective etching of films of gold patterned with micrometer-scale regions of monolayers of $CH_3(CH_2)_{15}S$ and $HO(CH_2)_2S$ forms microwires of gold supported on glass. These supported microwires function as microelectrodes.

The procedures we report for preparing microelectrodes of gold are general, do not require photolithography, and can be followed in any wet chemical laboratory. The bare gold surfaces of the electrodes can be functionalized with redox-active species and redox catalysts, making this method of preparation well-suited for the rapid prototyping of sensors and devices. Because the sequence of micromachining and selective deposition of SAMs on machined regions of gold can be performed repeatedly on the same sample, the procedures reported in this paper can be used to form surfaces with multiple, spatially-separated, microscopic areas each functionalized with a different surface-confined species. This capability, we believe, will make this procedure a useful one for fabricating structures with more than one surface-confined species.

Results and Discussion

Fabrication of Microelectrodes. The fabrication of three types of microelectrodes is described below; the procedures are detailed in the Experimental Section. All potentials are referenced to a saturated calomel electrode (SCE), unless indicated otherwise.

A. "Groove" Electrodes. "Groove" electrodes were formed by using the tip of a surgical scalpel blade to machine micrometer-wide grooves into a film of gold supporting a SAM of $CH_3(CH_2)_{15}S$ (Figure 1). Gold exposed by machining formed the electrochemically active surface of the microelectrode. Figure 2a is a scanning electron micrograph (SEM) of an array of grooves. Arrays of grooves (10 grooves × 10 grooves), rather than a single

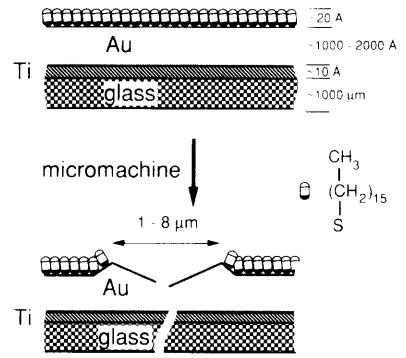

Figure 1. Schematic illustration of the procedure used to fabricate micrometer-wide electrodes of gold (groove electrodes): Au, evaporated film of gold; Ti, evaporated film of titanium used to promote the adhesion between the gold and glass microscope slide.

groove, were used to increase the magnitude of the current coming from them relative to the background currents (i.e., it improved the ratio of signal to noise). Each groove had a macroscopic length (~1 cm), width of ~1 μm, and depth of ~0.05 μm (Figure 2c).[9] The distance between parallel grooves was 500−1000 μm. Figure 2b shows an SEM of the intersection of two ~1-μm-wide grooves. Arrays of grooves with widths of ~8 μm were also prepared (Figure 2d) by machining the SAM with a larger load applied to the machine tip (see Experimental Section).

Cyclic voltammetry in aqueous solutions of 0.1 M H_2SO_4 was used to estimate the effective surface area of electrochemically active gold in the grooves (Figure 3).[15,17-19] Figure 3a shows a cyclic voltammogram measured using a macroscopic, polycrystalline film of gold (~1 cm^2); the anodic current begins at +1.1 V and is the sum of a small peak (shoulder) at +1.15 V and a large peak at +1.26 V. The presence of two peaks, and their relative sizes and positions, is similar to the two-electron oxidation of single-crystal Au(111)[28] immersed in an aqueous solution of either 0.1 M H_2SO_4[29] or 0.05 M H_2SO_4.[30] Because the anodic currents are probably convolved with a contribution from the oxidation of water, the areas of the anodic peaks are not reliable for estimating the effective surface area of gold on the film.[15,17,18] The cathodic peak at +0.87 V corresponds to the reduction of the surface layer of gold oxide to gold, and is used below to estimate the area of bare gold on the surface of the film.

The small size of the peak seen in the cyclic voltammogram of Figure 3b indicates that electrochemical oxidation of the gold film was essentially suppressed by the formation of a SAM of $CH_3(CH_2)_{15}S$ on its surface. From the relative areas of the cathodic peaks in Figure 3a,b, the effective surface area of electrochemically active gold on the SAM-covered surface was estimated to be 0.01% of the surface area of the gold film before the SAM was formed (Table 1). Because applied electrical potentials in aqueous solution can disrupt sulfur−gold bonds, this estimate of the effective area of bare gold can include a contribution caused by the method of measurement and should, therefore, be considered an upper bound.[19]

The potential for reduction of gold oxide on a gold film supporting a SAM of $CH_3(CH_2)_{15}S$ was 50 mV more negative than that measured using the macroscopic

(13) *X-ray-induced damage*: Bain, C. D. Ph.D. Thesis, Harvard University, 1988. Laibinis, P. E.; Graham, R. L.; Biebuyck, H. A.; Whitesides, G. M. *Science (Washington, D.C.)* **1991**, *254*, 981.

(14) *Electron transfer*: Porter, M. D.; Bright, T. B.; Allara, D. L.; Chidsey, C. E. D. *J. Am. Chem. Soc.* **1987**, *109*, 3559. Chidsey, C. E. D.; Bertozzi, C. R.; Putvinski, T. M. *J. Am. Chem. Soc.* **1991**, *112*, 4301. Hickman, J. J.; Ofer, D.; Zou, C. F.; Wrighton, M. S.; Laibinis, P. E.; Whitesides, G. M. *J. Am. Chem. Soc.* **1991**, *113*, 1128.

(15) Sabatani, E.; Rubinstein, I. *J. Phys. Chem.* **1987**, *91*, 6663.

(16) Finklea, H. O.; Hanshew, D. D. *J. Am. Chem. Soc.* **1992**, *114*, 3173.

(17) Finklea, H. O.; Avery, S.; Lynch, M.; Furtsch, T. *Langmuir* **1987**, *3*, 409.

(18) Sabatani, E.; Rubinstein, I.; Maoz, R.; Sagiv, J. *J. Electroanal. Chem.* **1987**, *219*, 365.

(19) Chidsey, C. E. D.; Loiacono, D. N. *Langmuir* **1990**, *6*, 682.

(20) Miller, C.; Cuendet, P.; Grätzel, M. *J. Phys. Chem.* **1991**, *95*, 877.

(21) Miller, C.; Grätzel, M. *J. Phys. Chem.* **1991**, *95*, 5225.

(22) Becka, A. M.; Miller, C. J. *J. Phys. Chem.* **1993**, *97*, 6233.

(23) Becka, A. M.; Miller, C. J. *J. Phys. Chem.* **1992**, *96*, 2657.

(24) The composition of the surface is probably a mixture of $CH_3(CH_2)_{15}SAu$ and $CH_3(CH_2)_{15}S(Au)_3$. For simplicity, we denote the surface-bound species as $CH_3(CH_2)_{15}S$.

(25) We use the term "bare gold" to describe the surface of gold on which the SAM was removed by micromachining: we expect the machined surface of the groove to adsorb adventitious organic material from the laboratory atmosphere.

(26) We use the term "micromachining" to mean the moving of metal by mechanical means rather than by chemical etching.

(27) The fabrication of 5 μm × 5 μm microelectrodes using the tip of a scanning tunneling microscope to modify SAMs of $CH_3(CH_2)_{15}S$ supported on gold has been recently reported: Ross, C. B.; Sun, L.; Crooks, R. M. *Langmuir* **1993**, *9*, 632.

(28) The evaporated films as prepared are polycrystalline but with predominant (111) orientation: Chidsey, C. E. D.; Loiacono, D. N.; Sleator, T.; Nakahara, S. *Surf. Sci.* **1988**, *200*, 45. Nuzzo, R. G.; Fusco, F. A.; Allara, D. L. *J. Am. Chem. Soc.* **1987**, *109*, 2358.

(29) Angerstein-Kozlowska, H.; Conway, B. E.; Hamelin, A.; Stoicoviciu, L. *J. Electroanal. Chem.* **1987**, *228*, 429.

(30) Štrbac, S.; Adžić, R. R.; Hamelin, A. *J. Electroanal. Chem.* **1988**, *249*, 291.

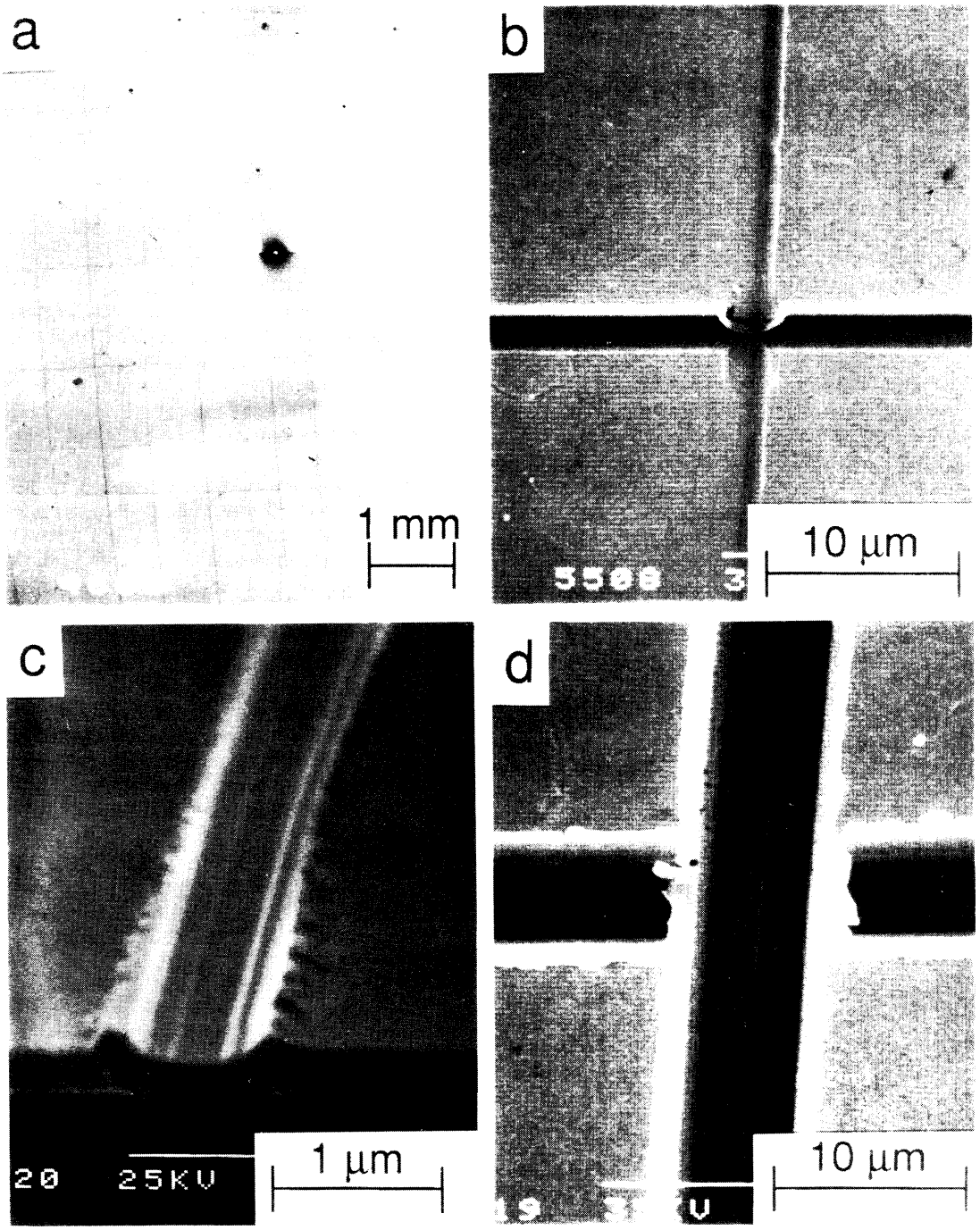

Figure 2. Scanning electron micrographs (SEMs) of micrometer-wide grooves of bare gold machined into a gold film covered with a SAM of $CH_3(CH_2)_{15}S$. (a) An array of 1-μm-wide grooves. The dark spot in the center of the image was caused by a contaminating particle on the surface of the gold film. The accelerating voltage (V_a) was 20 kV. (b) Top view of the intersection of two ~1-μm-wide grooves (V_a = 35 kV). (c) A cross-sectional view of a micrometer-wide groove. The gold film was supported on a wafer of silicon that was fractured normal to the groove for imaging (V_a = 25 kV). (d) The intersection of two 8-μm-wide grooves that were part of an array (not shown) (V_a = 35 kV).

Table 1. Voltammetric Peak Potentials and Geometric Areas of Electrodes in Aqueous 0.1 M H_2SO_4 Electrolyte[a]

electrode[b]	geometric area[c]	$E_{p,a}$ (V vs SCE) for oxidation of Au	$E_{p,c}$ (V vs SCE) for reduction of gold oxide
bare Au	1 cm^2	+1.15; +1.26	+0.87[d]
Au + $CH_3(CH_2)_{15}S$	10 000 μm^2	*e*	+0.82
array of 1-μm grooves	90 000 μm^2	+1.10 (shoulder); +1.20	+0.87
wire	11 000 μm^2	+1.17	+0.83

[a] Data obtained at a scan rate of 0.1 V/s. [b] Attempts to obtain the voltammetric behavior of gap electrodes in aqueous 0.1 M H_2SO_4 were unsuccessful. The electrodes were displaced from the supporting glass substrate during cyclic voltammetry. [c] Determined from the ratio of the area of the peak for the reduction of gold oxide at the designated electrode to that at a nominal 1 cm^2 bare gold electrode. [d] The area of the gold oxide reduction peak indicates a surface roughness (based on a two-electron reduction of a single-crystal Au(111) surface equal to 444 $\mu C/cm^2$)[30] of ~2.7 for the evaporatively deposited Au film electrode. [e] A well-defined oxidation process was not seen (Figure 3a).

surface of gold (Figure 3 and Table 1). Because both the oxidation of gold underlying a SAM and subsequent reduction of gold oxide so formed require the permeation of the SAM by water and ions, and because the SAM is hydrophobic and has a low dielectric constant, it is reasonable that the potentials for both redox processes

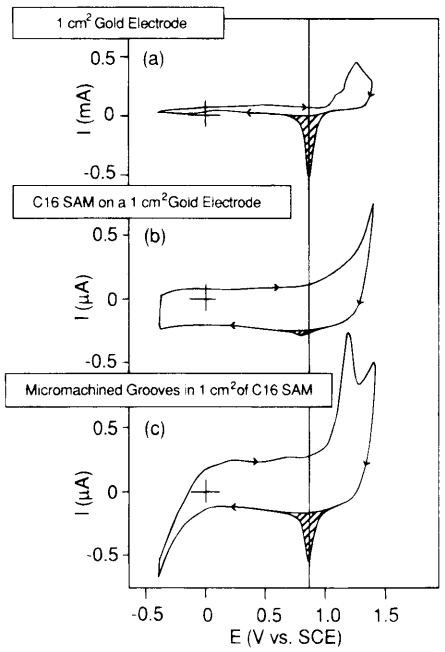

Figure 3. Cyclic voltammograms measured in aqueous solutions of 0.1 M H_2SO_4: (a) a macroscopic film of gold evaporated on a glass microscope slide (~1 cm^2); (b) a film of gold covered with a SAM of $CH_3(CH_2)_{15}S$ (~1 cm^2); (c) an array of micrometer-wide grooves micromachined into a film of gold covered with a SAM of $CH_3(CH_2)_{15}S$ (same sample as middle cyclic voltammogram). The potential was scanned at 100 mV/s. Note the different scales on the current axes. The cathodic currents (shaded) correspond to the reduction of surface layers of gold oxide to gold, and were used to estimate the area of electrochemically active gold on the surface of the films. The continuous and vertical line passing through the cathodic peaks is positioned at 0.87 V.

shift to more positive (oxidizing) and negative (reducing) values, respectively, as compared to the same processes on bare gold.

The capacitance of the SAM of $CH_3(CH_2)_{15}S$ on gold was estimated from Figure 3b using eq 1, where C is the capacitance ($\mu F/cm^2$) and Δq is the accumulation of charge ($\mu C/cm^2$) caused by a change in electrical potential ΔE (V). For a change in potential from −0.125 to +0.125 V

$$C = \Delta q/\Delta E \quad (1)$$

(ΔE = 0.25 V), the capacitive charge, Δq, at the surface of the SAM-modified gold was measured from Figure 3b to be 0.11 $\mu C/cm^2$. The capacitance calculated from eq 1 was 0.44 $\mu F/cm^2$. Chidsey and Loiacono[19] report the capacitance of a SAM of $CH_3(CH_2)_9S$ immersed in 0.1 M NaF to be 1.6 $\mu F/cm^2$. Assuming a model for the interface in which the capacitance is inversely proportional to the number of carbons in the alkane,[19] and using the value of capacitance reported by Chidsey and Loiacono[19] for the monolayer of $CH_3(CH_2)_9S$ (1.6 $\mu F/cm^2$), we calculated the capacitance of a monolayer of $CH_3(CH_2)_{15}S$ to be 1.0 $\mu F/cm^2$.[31] This value is approximately twice that measured from Figure 3b. Several factors can plausibly contribute to the differences between the measured and estimated capacitance: the nature of electrolytes (aqueous NaF vs aqueous H_2SO_4; the hydrophobic SAM is probably less permeable to the divalent than monovalent anions), and the degree of order within the SAM (SAMs of $CH_3(CH_2)_{15}S$ have been shown to be more ordered than SAMs of $CH_3(CH_2)_9S$;[10] we expect, therefore, that water and ions will permeate less into SAMs of $CH_3(CH_2)_{15}S$ than $CH_3(CH_2)_9S$).

Figure 3c shows a cyclic voltammogram measured using an array of grooves (10 rows × 10 columns) machined into a SAM of $CH_3(CH_2)_{15}S$. The shape and positions of the anodic peaks corresponding to the oxidation of the machine-exposed gold within the grooves have changed relative to those obtained for the evaporated film of gold (Figure 3a). This change is plausibly caused by the exposure of different facets of gold on the surface of the machined groove as compared to the evaporated surface of predominantly Au(111). The prominent anodic peak at 1.20 V seen in Figure 3c and the slight shoulder at ~1.1 V are consistent with oxide formation on a Au(100) surface in 0.05 M H_2SO_4.[30] If a (111) crystallographic plane is cut open, (100) facets should be exposed. The electrochemically active surface area of gold in the array of micromachined grooves was estimated to be 0.09% of that present on the 1 cm^2 of bare gold (from relative areas of the cathodic peaks). Knowing the total length of the grooves (~20 cm), and assigning a planar band geometry to the micromachined groove, we calculated the effective width of electrochemically active gold in the micromachined grooves to be ~0.5 μm. This value is slightly smaller than the width of deformed gold seen in the SEM (~1 μm; see Figure 2b). The disagreement between the widths of the grooves obtained by the two methods is not unreasonable because some fraction of the area of the deformed gold in and around the micromachined grooves is probably still covered by SAM and because the surface of the grooves can consist of less densely packed planes of Au than Au(111).

Upon scanning negative of 0 V with the grooved array, an increase in cathodic current was observed (Figure 3c), unlike the response for either bare Au (Figure 3a) or Au supporting a SAM of $CH_3(CH_2)_{15}S$ (Figure 3b). Because the onset of the cathodic current observed in Figure 3c was displaced to −0.8 V at pH 7 (not shown), and because a comparable reduction of protons at the bare Au at these potentials does not appear to be occurring at comparable current densities, the process(es) giving rise to the current appear related to a proton-dependent reduction involving remnants of a SAM in the groove. Alternatively, exposed facets of gold other than Au(111) could be mediating the process leading to the cathodic current as the kinetics for proton electroreduction are slower at Au(111) relative to the other gold surfaces.[32]

B. "Wire" Electrodes. "Wire" electrodes were prepared using the three-step procedure shown in Figure 4. First, micrometer-wide grooves of bare gold were machined into a film of gold supporting a monolayer of $HO(CH_2)_2S$. Second, the machined grooves of gold were covered selectively with SAMs of $CH_3(CH_2)_{15}S$. Third, the areas of the gold film covered with $HO(CH_2)_2S$ were etched selectively with an aqueous solution of CN^- that was saturated with O_2.[8,33] This procedure was used to fabricate wires supported on glass with widths of ~1 μm, lengths of ~1 cm, and top surfaces covered with SAMs of $CH_3(CH_2)_{15}S$. The fabrication of wire electrodes relies on two

(31) The capacitance of the SAM of $CH_3(CH_2)_{15}S$ can also be estimated using $C = \epsilon\epsilon_0/d_{eff}$, where ϵ = 2.26 (the value for polyethylene), $\epsilon_0 = 8.854 \times 10^{-14}$ F/cm, and $d_{eff} = 2.3 \times 10^{-7}$ cm (assuming the alkane chain is fully extended and tilted 30° from the normal).[10] The capacitance calculated is 0.87 $\mu F/cm^2$, in close agreement with the value estimated from ref 19 (see text).

(32) Hamelin, A.; Weaver, M. J. *J. Electroanal. Chem.* **1987**, *223*, 171.

(33) The etchant was an aqueous solution of 0.1 M KCN and 1 M KOH, saturated with O_2, and stirred vigorously. A 250-Å-thick film of gold supporting a monolayer of $HO(CH_2)_2S$ was etched in 5–10 min, and 1000-Å-thick gold films were etched in ~45–60 min. Monolayers of $HO(CH_2)_2S$ were partially displaced from the surface of the gold film by immersion in an ethanolic solution of $CH_3(CH_2)_{15}SH$ for times longer than ~30 s. Accompanying the displacement reaction was an increase in the time required to etch the film of gold.

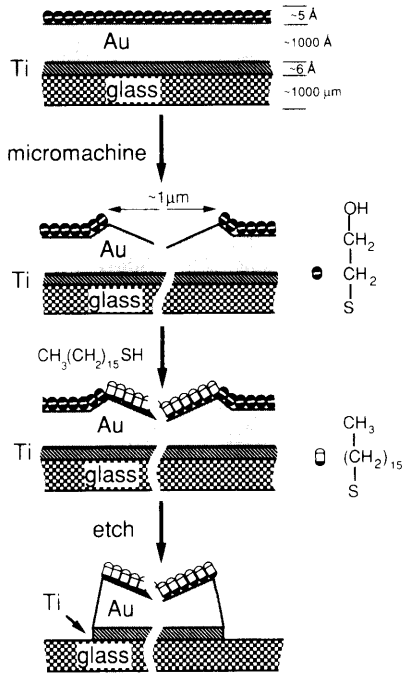

Figure 4. Schematic illustration of the procedure used to form micrometer-wide wires of gold supported on glass (microwire electrodes) using micromachining, SAMs, and wet chemical etching: Au, evaporated film of gold; Ti, evaporated film of titanium used to promote the adhesion between the gold and glass microscope slide.

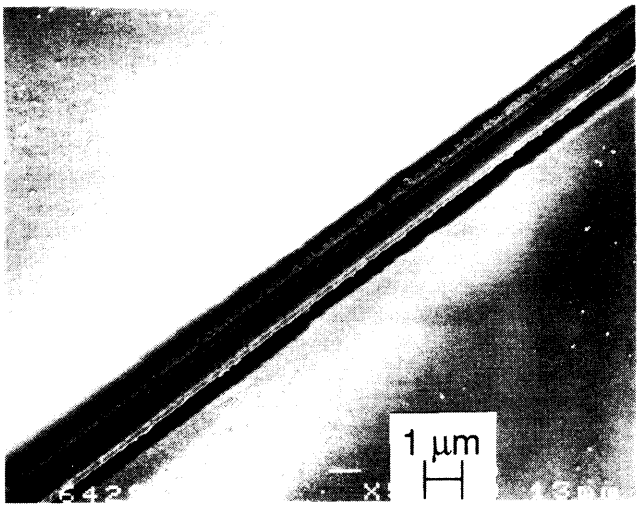

Figure 5. Scanning electron micrograph of a 1-μm-wide, gold wire electrode supported on glass. The bright areas in the SEM are caused by the electrical charging of the glass microscope slide. The wire is surrounded by a dark halo that is caused, we believe, by "spillover": the conducting wire can relax the buildup of electrical charge on the neighboring surface of the glass slide. The accelerating voltage was 5 kV.

properties of monolayers of $HO(CH_2)_2S$. First, monolayers of $HO(CH_2)_2S$ supported on gold films are not completely displaced by $CH_3(CH_2)_{15}S$ when exposed to concentrated ethanolic solutions of $CH_3(CH_2)_{15}SH$ for less than 1 min. Second, films of gold-supporting monolayers of $HO(CH_2)S$ briefly exposed to $CH_3(CH_2)_{15}SH$ can be readily etched by aqueous solutions of CN^- saturated with O_2.[33] In contrast, a monolayer of $CH_3(CH_2)_{15}S$ protects an underlying film of gold from etching.[8]

Figure 5 is a SEM of a section of a 1-μm-wide × 100-nm-thick × 13-mm-long supported wire electrode. The wires were connected at either one or both ends to macroscopic areas of SAM-covered gold film for the purpose of making electrical contact (see Experimental Section).

The area of electrochemically active gold on the supported wire (relative to bare Au) was estimated to be 11 000 μm^2 using cyclic voltammetry in an aqueous solution of 0.1 M H_2SO_4, as described above (Table 1). Assuming the electrochemically active surface of gold to be the walls of the wire (the top of the wires is covered with a SAM of $CH_3(CH_2)_{15}S$), we calculated the geometric area of exposed gold to be 2 × 0.1 μm × 13 mm = 2600 μm^2 (0.1 μm corresponds to the height of the walls of the wire, and 13 mm corresponds to the length of the wire electrode). The measured electrochemically active surface area of the electrode is larger, by a factor of 4, than the calculated surface area of the walls. Possible explanations for the difference between the estimates include exposed gold on the top surface[34] of the supported wire and roughness on the edges and faces of the wire (see Figure 5) caused by the etch procedure (which would lead to greater electrochemically active area than anticipated on the basis of the calculations of geometric area).

C. "Gap" Electrodes. "Gap" microelectrodes were prepared from supported wire electrodes connected at both ends to electrical contact pads (see above description for the preparation of supported wire electrodes). First, exposed gold surfaces of the wire were covered with a SAM of $CH_3(CH_2)_{15}S$. To form an electrically insulating SAM of $CH_3(CH_2)_{15}S$ on the walls of the wires, it was necessary to clean the wires electrochemically by cycling the potential of the wires between −0.4 and 1.4 V in an aqueous solution of 0.1 M H_2SO_4 prior to immersing the wires in an ethanolic solution of $CH_3(CH_2)_{15}SH$. We attributed the necessity of the pretreatment to poisoning of the Au surface by strongly adsorbed CN^-, which, unlike adventitious adsorbates on Au, did not appear to be completely displaced by the thiol moiety.[35] Second, a 1-μm-wide gap was machined into the wire using the tip of a surgical scalpel as the machining tool (Figure 6). The machine-exposed areas of gold on either side of the gap were used as working and counter electrodes. The geometry of the gap varied from one sample to another. Residual material (probably gold machined from the gap) was sometimes observed by scanning electron microscopy to be deposited on either side of the gap as shown in Figure 6a. Although this residual material was not always present, as seen in Figure 6b, holes that formed during the etching of the film of gold can be observed in the wire by scanning electron microscopy.

Electrochemical Characterization of Microelectrodes. We measured cyclic voltammograms using groove, wire, and gap electrodes in aqueous solutions of $K_3Fe(CN)_6$, $K_4Fe(CN)_6$, and $Ru(NH_3)_6Cl_3$ and solutions of acetonitrile containing ferrocene. Figure 7 is a schematic illustration of the experimental setup used to measure the cyclic voltammograms of these electrodes. Details are presented in the Experimental Section. The voltammetric data obtained from these studies are summarized in Table 2.

A. Groove Electrodes. The cyclic voltammogram shown in Figure 8a was measured using a macroscopic film of gold (~0.2 cm^2) immersed in an aqueous solution of 1 mM $K_3Fe(CN)_6$, 10 mM K_2HPO_4 (pH 7.0), and 0.1 M $NaClO_4$. The cathodic peak ($E_{p,c}$ = 0.13 V) corresponds to the reduction of $Fe(CN)_6^{3-}$ to $Fe(CN)_6^{4-}$. The peak-to-peak separation of the cathodic and anodic waves was ~70 mV. The cathodic peak current ($i_{p,c}$) was measured as a function of the scan rate (ν) for scan rates between 10 and 100 mV/s: current and rate were related by the

(34) The calculated geometric area of the top surface of the wire is ~1 μm × 13 mm = 13 000 μm^2.

(35) Abbott, N. L.; Whitesides, G. M. Unpublished results.

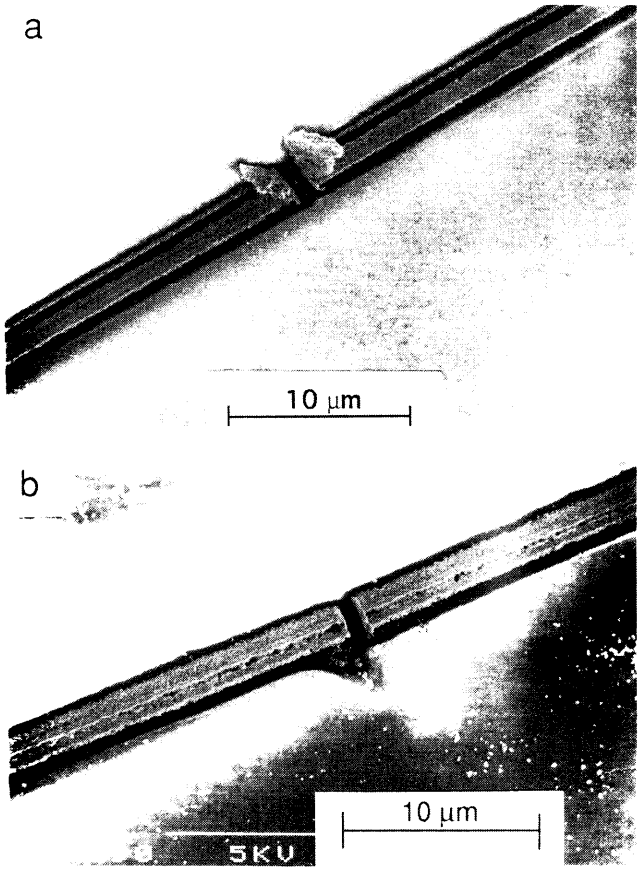

Figure 6. Scanning electron micrographs of gap electrodes. (a) A ~1-μm-wide gap machined into a ~1-μm-wide supported wire of gold. Note that, in addition to the ~1-μm-wide supported wire of gold, a ~0.1-μm-wide wire that runs parallel to the 1-μm-wide wire is visible in (a); the two wires are separated by ~300 nm. The residual material at the end of each electrode is probably gold that was machined from the gap. This gold may contribute to the working area of the electrode. (b) An approximately 1-μm-wide gap machined into a 1-μm-wide wire. At this magnification holes are visible in the wires. The accelerating voltage was 5 kV in both images.

power law $i_p \sim \nu^{0.45}$. The exponent of ν contains information about the nature of the mass transport at the electrode. For a surface-confined, nondiffusing redox solute, an exponent of 1 is obtained. When semi-infinite (planar) diffusion controls mass transport, the exponent is 0.5 (i_p is proportional to $\nu^{1/2}$). When finite diffusion describes the mass transport of the electroactive solute, as has been observed for polymer-modified electrodes, an exponent between 0.5 and 1.0 is obtained. When nonplanar (spherical or cylindrical) diffusion describes the mass transport (as occurs for microelectrodes), the exponent falls below 0.5. For hydrodynamic voltammetry, as at rotated disk electrodes, the limiting current is essentially independent of scan rate for the range of scan rates used here (10–100 mV/s); i.e., the exponent is zero. The exponent of 0.45 measured using a macroscopic Au electrode is close to 0.5 as expected for planar diffusion of a redox-active species to an electrode.[1,2]

Figure 8b shows a cyclic voltammogram measured using a gold surface (1 cm^2) supporting a SAM of $CH_3(CH_2)_{15}S$ immersed in the same solution of electrolyte and $Fe(CN)_6^{3-}$. The SAM of $CH_3(CH_2)_{15}S$ effectively blocks the transfer of electrons between the surface of the gold electrode and the $Fe(CN)_6^{3-}$ species in aqueous solution (as seen by the negligible current flowing at the formal potential for this redox species).

A small cathodic current of 0.25 μA was observed at a potential of −0.1 V; the form of the $i-E$ curve in this region

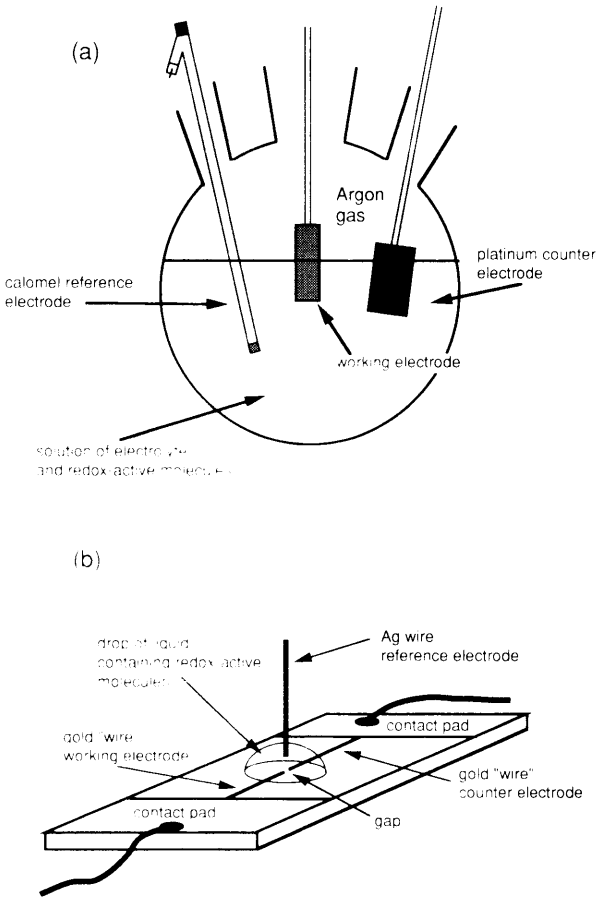

Figure 7. Schematic illustrations of the experimental apparatus for cyclic voltammetry: (a) groove and wire electrodes; (b) gap electrodes. The volume of the drop was typically 10–20 μL. A detailed description is given in the Experimental Section.

Table 2. Voltammetric Peak Potentials and Currents of Groove and Wire Electrodes in Aqueous Solutions of $Fe(CN)_6^{3-}$ and Ferrocene in Acetonitrile

electrode	half-wave potential (V vs SCE)	i_p (or i_{lim}) at 50 mV/s	calcd i_p (or i_{lim}) from eq 5
Reduction of $Fe(CN)_6^{3-}$, pH 7, 0.1 M $NaClO_4$ in Water			
bare Au	+0.17	60 μA	not calcd[a]
array of grooves			
1 μm	+0.18	3 μA	6.5 μA
8 μm[b]	+0.18	9 μA	8.3 μA
wire		32 nA	330 nA
Ferrocene in 0.1 M Bu_4NPF_6/CH_3CN			
wire	0.40	1000 nA	1400 nA
$Ru(NH_3)_6^{3+}$, pH 7, 0.1 M $NaClO_4$ in Water[b]			
array of grooves			
8 μm	−0.20[c]	−15 μA	−18 μA

[a] The area of the macroscopic electrode is only known approximately (~0.2 cm). We cannot, therefore, make a quantitative comparison between experiment and calculation. [b] The scan rate was 10 mV/s. [c] The separation of the peaks was 60 mV.

suggests a limitation to the rate of transfer of electrons through the SAM (or defects in the SAM) to the electrode (see Figure 3b), rather than a diffusion-limited current.

The current arising from heterogeneous transfer of electrons can be described by the Butler–Volmer equation,[36]

$$i = nFAk^\circ(c_o e^{-\alpha nf(E-E^{o\prime})} - c_r e^{(1-\alpha)nf(E-E^{o\prime})}) \qquad (2)$$

where n is the moles of charge transferred per mole of

(36) Bard, A. J.; Faulkner, L. R. *Electrochemical Methods*; Wiley: New York, 1980; pp 100–112.

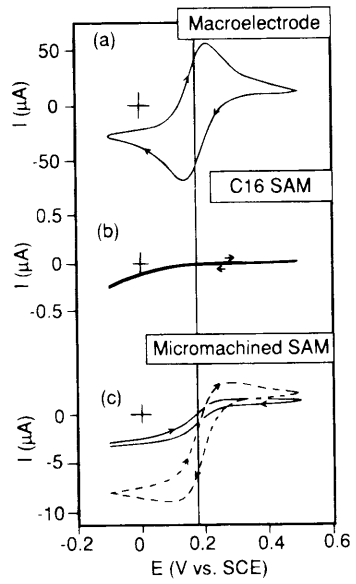

Figure 8. Cyclic voltammograms measured in aqueous solutions of 1 mM $K_3Fe(CN)_6$, 10 mM K_2HPO_4 (pH 7.0), and 0.1 M $NaClO_4$: (a) macroscopic film (~0.2 cm^2) of gold evaporated onto a glass microscope slide (50 mV/s); (b) film of gold (~1 cm^2) covered with a SAM of $CH_3(CH_2)_{15}S$ (10 mV/s); (c) arrays of micrometer-wide grooves machined into a SAM of $CH_3(CH_2)_{15}S$ (see Figure 2a and the accompanying text for details). The dotted line corresponds to an array of 8-μm-wide grooves (scanned at 10 mV/s), and the continuous line corresponds to an array of 1-μm-wide grooves (scanned at 50 mV/s).

redox species arriving at the surface of the electrode (n = 1), F is the Faraday constant, A is the area of the electrode, $k°$ is the standard rate constant for the process of heterogeneous electron transfer, c_o and c_r are the concentrations of the oxidized and reduced forms of the redox-active species at the surface of the electrode (these concentrations are equal to the bulk concentrations in the absence of mass transport limitations), α is the transfer coefficient (defined below), $f = F/RT$, T is temperature, E is the potential of the electrode, and $E°'$ is the formal reduction potential of the redox-active species. The transfer coefficient can be understood as follows: for an electrochemical process at an electrode with a free energy of activation of ΔG_a at E = 0 V, a change in the potential of the electrode causes a change in the activation free energy of αnFE.[36] For solutions containing only oxidized ($c_r = 0$) or reduced ($c_o = 0$) forms of the redox species, eq 2 can be simplified to eqs 3 and 4. We have used eq 3 to

$$i_o = nFAk°c_o e^{-\alpha nf(E-E°')} \qquad c_r = 0 \qquad (3)$$

$$i_r = -nFAk°c_r e^{(1-\alpha)nf(E-E°')} \qquad c_o = 0 \qquad (4)$$

analyze the cathodic current in Figure 8b. A transfer coefficient (see eq 3) of 0.18 and an apparent heterogeneous rate constant of 5.6×10^{-7} cm/s were obtained from a Tafel plot (not shown) of the data. These values are in approximate agreement with measurements reported by Miller and co-workers[20] for SAMs of $HO(CH_2)_{16}S$ and $Fe(CN)_6^{3-}$ in 0.1 M KCl; these authors report a transfer coefficient of 0.2 and an apparent heterogeneous rate constant of 1.3×10^{-7} cm/s.[37]

Grooves micromachined in the SAM caused an increase in Faradaic current relative to that passed at gold covered with a SAM of $CH_3(CH_2)_{15}S$, as seen by the cyclic voltammograms of Figure 8c. Both cyclic voltammograms have sigmoidal shapes, in contrast to Figure 8a which has the well-defined anodic and cathodic peaks characteristic of (semi-infinite) diffusion-controlled electron transfer at a macroscopic electrode. The limiting cathodic current (i_{lim}) for the array of 8-μm-wide grooves was measured as a function of the scan rate between 10 and 100 mV/s: the obtained exponent of 0.12 ($i_{lim} \sim \nu^{0.12}$) indicates that mass transport to the microgroove electrodes is more rapid than mass transport to the macroscopic electrodes and can no longer be described by planar diffusion (see above).

The cyclic voltammogram measured using the array of 1-μm-wide grooves was obtained after the surfaces of the grooves were electrochemically conditioned by cycling the potential between −0.4 and +1.4 V in an aqueous solution of 0.1 M H_2SO_4. If this procedure was not performed, the plateau in current at negative potentials was generally less pronounced than that shown in Figure 8c: the cathodic current increased monotonically with more negative potentials. This electrochemical behavior was reversed in aqueous solutions of $Fe(CN)_6^{4-}$: no current was measured at negative potentials, while a monotonic increase in anodic current was measured at positive potentials. The same samples did not show Faradaic currents in aqueous solutions of electrolyte without redox-active molecules. The cyclic voltammograms measured using arrays of 8-μm-wide grooves did not require electrochemical conditioning in aqueous solutions of 0.1 M H_2SO_4.

We interpret the absence of peaks and the presence of plateaus in the cyclic voltammograms measured using arrays of microgrooves to indicate a near-steady-state concentration of redox-active solutes was maintained in the film of liquid near the electrode (boundary layer) during the forward and reverse voltage scans. The limiting currents observed in Figure 8c were determined, we believe, by the maximum rate of mass transport of ions from bulk solution to the surface of the electrode.

Mass transport-limited currents, $i(t)$, at band-type microelectrodes can be estimated[38,39] using eqs 5 and 6, where τ is dimensionless time ($\tau = Dt/w^2$), t is time, w is the width of the band electrode, D is the diffusivity of the

$$\frac{i(t)}{nFDc_oL} = \frac{\pi e^{-2(\pi\tau)^{1/2}/5}}{4(\pi\tau)^{1/2}} + \frac{\pi}{\ln[(64\pi e^{-\gamma})^{1/2} + e^{5/3}]} \qquad \tau > 2/5 \quad (5)$$

$$\frac{i(t)}{nFDc_oL} = \frac{1}{(\pi\tau)^{1/2}} + 1 \qquad \tau < 2/5 \qquad (6)$$

redox-active species, c_o is the bulk concentration of redox-active species, L is the length of the band electrode, and $\gamma = 0.577$. Equations 5 and 6 are approximate and have been found to agree with numerical simulations to within 1.3%.[38,39] For an array of 20 grooves, each 1 μm wide ($w = 1 \times 10^{-4}$ cm), 1 cm long ($L = 20 \times 1$ cm = 20 cm), and contacting a 1 mM solution of $Fe(CN)_6^{3-}$ ($D = 6.1 \times 10^{-6}$ cm^2/s,[18] $c_o = 1 \times 10^{-6}$ mol/cm^3), we calculate $\tau = 2440$ and, using eq 5, $i(t = 4\ s) = 6.5\ \mu A$.[40] In comparison, the experimentally measured current was ~3 μA (Figure 8c

(37) Miller *et al.*[20] used SAMs formed from aqueous solutions of 16-mercaptohexadecanol (in the presence of a cationic surfactant); the rate constants were measured at scan rates of 50 V/s in aqueous solutions of 0.1 M KCl. Factors such as the type and concentration of electrolyte,[21] the nature of the head group of the SAM,[22] and the rate at which the potential is scanned[23] have been reported to influence the apparent rate constants. All these factors can plausibly contribute to the difference in the value of the rate constants measured by us and by Miller *et al.*[20]

(38) Coen, S.; Cope, D. K.; Tallman, D. E. *J. Electroanal. Chem.* **1986**, *215*, 29.

(39) Bard, A. J.; Crayston, J. A.; Kittlesen, G. P.; Shea, T. V.; Wrighton, M. S. *Anal. Chem.* **1986**, *58*, 2321.

(40) Four seconds corresponds to the time taken to scan the potential 200 mV (from 0.2 to 0.4 V in Figure 8c) at 50 mV/s.

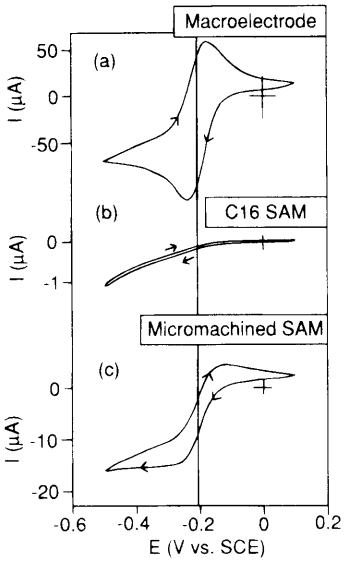

Figure 9. Cyclic voltammograms measured in aqueous solutions of 2 mM $Ru(NH_3)_6Cl_3$, 10 mM K_2HPO_4 (pH 7.0), and 0.1 M $NaClO_4$: (a) macroscopic film (~0.2 cm^2) of gold evaporated onto a glass microscope slide (50 mV/s); (b) film of gold (~1 cm^2) covered with a SAM of $CH_3(CH_2)_{15}S$ (10 mV/s); (c) array of 8-μm-wide grooves machined into a SAM of $CH_3(CH_2)_{15}S$ (10 mV/s).

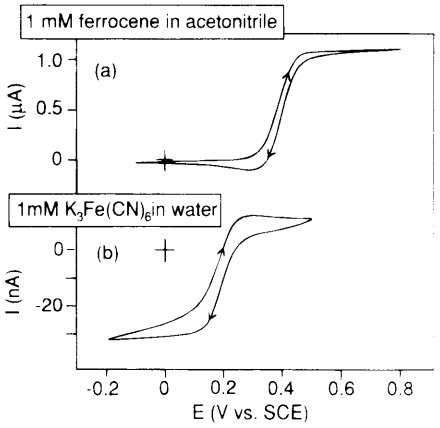

Figure 10. Cyclic voltammograms of a wire electrode (100 nm × 13 mm × 1 μm; shown in Figure 5): (a) 1 mM ferrocene, 0.1 M TBAPF in acetonitrile; (b) aqueous solution of 1 mM $K_3Fe(CN)_6$, 10 mM K_2HPO_4 (pH 7.0), and 0.1 M $NaClO_4$. The potential was scanned at 50 mV/s. Note the different scales of current on the vertical axes.

and Table 2). The smaller value of the measured current as compared to the calculated current is consistent with our earlier estimation that a fraction of the surface area of the groove was electrochemically inactive in 0.1 M H_2SO_4. For the array of 8-μm-wide grooves we calculated $\tau = 190$ and, using eq 5, $i(t = 20\ s) = 8.3\ \mu A$. In comparison, the experimentally measured current was 9 μA (Figure 8c and Table 2).

Cyclic voltammograms measured using 8-μm-wide grooves in an aqueous solution of 2 mM $Ru(NH_3)_6Cl_3$ (Figure 9) showed features similar to those of voltammograms in $Fe(CN)_6^{3-}$ (Figure 8). The limiting current (−15 μA) measured in 2 mM $Ru(NH_3)_6Cl_3$ was in good agreement with the calculated (using $D = 7.1 \times 10^{-6}$ cm^2/s)[39] value (−18 μA; see Table 2).

B. Wire Electrodes. Figure 10 shows cyclic voltammograms measured using 1-μm-wide, supported wire electrodes (Figure 5). The cyclic voltammograms were measured (in order) using, first, a solution of acetonitrile containing 1 mM ferrocene and 0.1 M TBAPF ($[Bu]_4NPF_6$) and, second, an aqueous solution of 1 mM $Fe(CN)_6^{3-}$. The plateaus in current observed for both the oxidation of ferrocene in nonaqueous electrolyte and the reduction of ferricyanide in aqueous electrolyte are qualitatively consistent with microelectrode behavior.[1,2]

Self-assembled monolayers of $CH_3(CH_2)_{15}S$ do not block the transfer of electrons between gold electrodes and solutions of ferrocene in acetonitrile, in agreement with previous results by Finklea and co-workers.[17] The electrochemically active surface area of the electrode corresponds, therefore, to the entire surface area of the wire: the surface area of the walls and the top of the wire. By approximating the wire electrode as a 1-μm-wide band electrode, we used eq 5 to estimate the magnitude of the mass transport-limited current to its surface. We calculated $\tau = 6800$ and $i(t = 4\ s) = 1.1\ \mu A$ using parameter values $c_o = 1 \times 10^{-6}$ mol/cm^3, $D = 1.7 \times 10^{-5}$ cm^2/s,[41] $w = 1 \times 10^{-4}$ cm, and $L = 1.3$ cm. The limiting currents in Figure 10 are ~1.0 μA and agree with the calculated mass transport-limit currents.

Because self-assembled monolayers of $CH_3(CH_2)_{15}S$ do block the transfer of electrons between the surface of a gold electrode and an aqueous solution of $Fe(CN)_6^{3-}$ (Figure 8b), the working area of the supported wire electrode in an aqueous solution of $Fe(CN)_6^{3-}$ corresponds to the surface area of the vertical walls of the wires. We calculated the working area of the electrode by approximating the shape of the wire as a single, *horizontal* 0.2-μm-wide band electrode and used eq 5 to estimate the magnitude of the mass transport-limited current to the electrode.[42] Using eq 5 and $c_o = 1 \times 10^{-6}$ mol/cm^3, $D = 6.1 \times 10^{-6}$ cm^2/s,[18] $w = 0.2 \times 10^{-4}$ cm, and $L = 1.3$ cm, we calculated $\tau = 61\ 000$ and $i(t = 4\ s) = 330$ nA. The measured currents were ~32 nA (Figure 10), smaller by a factor of ~10 than the calculated current. The discrepancy between the calculated and measured currents may arise because eq 5 describes mass transport to a horizontal, planar electrode, whereas, in this electrode geometry, the walls of the supported wire are vertical with impermeable boundaries along their edges (i.e., the glass substrates). We suspect that the vertical geometry is less accessible to redox-active species in solution than the horizontal geometry assumed for the calculation of the current.

C. Gap Electrodes. Figure 7b is a schematic illustration of the experimental setup used to measure cyclic voltammograms of gap electrodes (see Figure 6). The machine-exposed gold on the end of one wire formed the working electrode, and the other machine-exposed end was used as the counter electrode. Cyclic voltammograms were measured by placing a 10−20-μL drop of aqueous solution (containing the redox-active species and electrolyte) on the gap and inserting a silver wire (reference electrode) into the drop.

Figure 11a is a cyclic voltammogram (measured in 1 mM $Fe(CN)_6^{3-}$) of a supported wire with all surfaces (walls and top of the wire) covered by SAMs of $CH_3(CH_2)_{15}S$. The measurement was performed before the gap was machined across the wire. The absence of measurable (<0.1 nA) Faradaic currents confirmed that the supported wire of gold was electrically insulated from the solution by the SAM of $CH_3(CH_2)_{15}S$. Parts b and c of Figure 11 are cyclic voltammograms measured after the gap was machined by using the tip of a surgical scalpel blade. The formation of the gap was detected initially by an increase in the

(41) Mirkan, M. V.; Richards, T. C.; Bard, A. J. *J. Phys. Chem.* **1993**, *97*, 7672.

(42) Mass transport-limited currents can also be calculated by approximating the walls of the wires as two independent ("electrically sinked") and planar 0.1-μm-wide band electrodes. This approximation leads to a calculated limiting current of 600 nA which is larger by a factor of ~20 than the measured current.

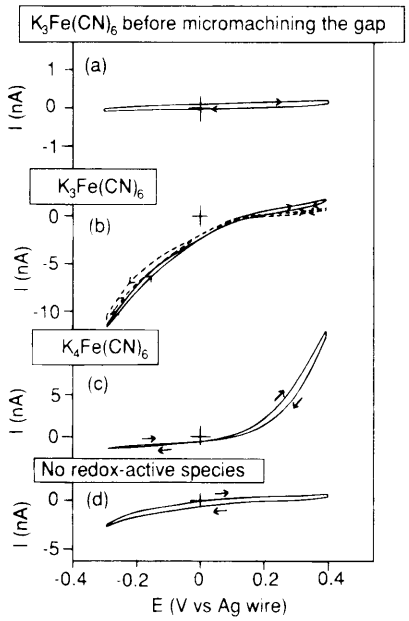

Figure 11. Cyclic voltammograms of gap electrodes in aqueous solutions of 1 mM $K_3Fe(CN)_6$ or 1 mM $K_4Fe(CN)_6$, 10 mM K_2HPO_4 (pH 7.0), and 0.1 M $NaClO_4$. (a) A supported wire electrode with walls and top surfaces covered with SAMs of $CH_3(CH_2)_{15}S$ (before machining the gap). The redox-active species in solution was $K_3Fe(CN)_6$; the scan rate was 200 mV/s. (b) Solid line, gap electrodes (one electrode was the working electrode, and the other was the counter electrode) scanned at 50 mV/s in an aqueous solution of $K_3Fe(CN)_6$; broken line, one electrode from the gap (working electrode) scanned at 200 mV/s in an aqueous solution of $K_3Fe(CN)_6$. The counter electrode was an external Pt wire. (c) Gap electrodes (one electrode was the working electrode, and the other was the counter electrode) in an aqueous solution of $K_4Fe(CN)_6$; the scan rate was 50 mV/s. (d) The same gap electrodes in aqueous electrolyte without redox-active species.

electrical resistance of the wire from 2450 Ω to >20 MΩ. The shape and size of the gap was determined *after* the electrochemical measurements by using scanning electron microscopy (Figure 6).[43] Cathodic currents (with $Fe(CN)_6^{3-}$, Figure 11b) and anodic currents (with $Fe(CN)_6^{4-}$, Figure 11c) increased by factors greater than 10 after machining the gap. Because the currents measured using the gap electrodes changed with the oxidation state of the redox-active species in the solution ($Fe(CN)_6^{3-}$ versus $Fe(CN)_6^{4-}$), and because cyclic voltammograms measured in the absence of redox-active species in solution (Figure 11d) showed smaller currents than in the presence of redox-active species, the currents measured in Figure 11b,c result, we believe, from the oxidation/reduction of $Fe(CN)_6^{4-/3-}$ at the surface of the gap electrodes. The shapes of the cyclic voltammograms differ, however, from the shapes of the cyclic voltammograms measured using groove electrodes (Figures 8 and 9) and wire electrodes (Figure 10) in that the voltammograms measured using the gap electrodes do not have peaks or plateaus in the anodic or cathodic currents. The $i-E$ shape obtained is reminiscent of that seen on gold coated with a SAM of $CH_3(CH_2)_{15}S$ (Figure 8b); the current measured at the gap electrodes can also be exponentially related to the overpotential $E - E^{\circ\prime}$ (Figure 12). Currents that result from kinetic limitations to electron transfer should be independent of the rate at which the potential is scanned: the current measured in Figure 11b changed by less than 3% when the scan rate was varied over the modest range of 50–200 mV/s.

(43) Self-assembled monolayers of $CH_3(CH_2)_{15}S$ supported on films of gold are damaged by exposure to the beam of electrons in a scanning electron microscope.[13]

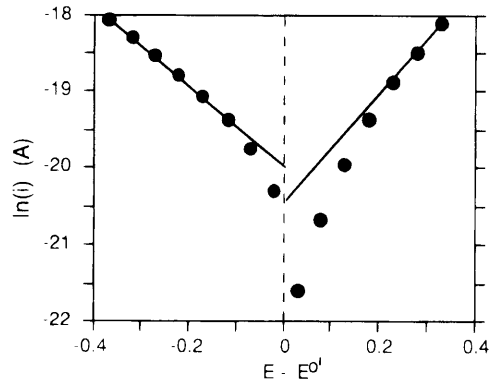

Figure 12. Tafel plot, $\ln(i)$ versus $E - E^{\circ\prime}$, using cyclic voltammograms in Figure 11 for gap electrodes measured in aqueous solutions of 1 mM $K_3Fe(CN)_6$ or 1 mM $K_4Fe(CN)_6$, 10 mM K_2HPO_4, and 0.1 M $NaClO_4$.

Because the mass flux to a disk or hemispherical electrode increases inversely with the radius of the electrode,[1,2] and because the rate of heterogeneous electron transfer is independent of the radius of the electrode, kinetic effects become the rate-determining step for small electrodes. The size of an electrode, r, corresponding to the crossover from mass transport-limited currents to kinetically limited currents can be estimated from $r \approx D/k^\circ$, where D is the diffusivity and k° is the standard rate constant for the heterogeneous electron transfer process.[1,2] For $Fe(CN)_6^{3-/4-}$ and gold electrodes ($D = 6.1 \times 10^{-6}$ cm²/s and $k^\circ = 1.0 \times 10^{-2}$ to 6.0×10^{-2} cm/s),[15,17,18] we estimated $r \approx D/k^\circ$ to range from 1 to 3 μm, a value that is comparable in magnitude to the size of the gap electrodes estimated from scanning electron microscopy (Figure 6). This calculation supports the hypothesis that the kinetics of electron transfer are important in determining the shape of the cyclic voltammograms obtained for gap electrodes, as seen in Figure 11. The electrochemically active area of the gap electrode was estimated from the experimentally observed currents by assuming the currents in Figure 11b,c to be governed by the rate of heterogeneous electron transfer (and not mass transport). Recent work by Smith and White indicates that at spherical electrodes with diameters $\sim \leq 0.1$ μm, the violation of electroneutrality—even in the presence of excess supporting electrolyte—can lead to the appearance of a kinetically limited wave shape even when the electrochemical reaction continues to be transport-limited.[44] We do, however, treat our data as indicative of kinetically limited currents and compare our results with previous reports.[17,18]

We have used eqs 3 and 4 to interpret the cyclic voltammograms shown in Figure 11. Figure 12 is a plot of $\ln(i)$ versus $E - E^{\circ\prime}$. The transfer coefficient was calculated from the slope of the plot, and the apparent, electrochemically active area of the electrode was calculated from the extrapolated intercept of the plot with the y axis. The results are summarized in Table 3.

The apparent radius of the electrode was calculated by assuming a hemispherical geometry and values for the heterogeneous rate constants between 1×10^{-2} and 6×10^{-2} cm/s.[15,17,18] Using the values of the intercept of the y axis in Table 3, our estimates of the apparent sizes of the electrodes, based on the above values of the heterogeneous rate constant, ranged between 2 and 6 μm. The apparent radii are similar to the size of the electrode estimated from SEMs (~2–3 μm; see Figure 6). This agreement, in addition to the general shape of the cyclic voltammograms, supports our view that the current at the gap electrode is influenced strongly by the rate of

(44) Smith, C. P.; White, H. S. *Anal. Chem.* **1993**, *65*, 3343.

Table 3. Apparent Transfer Coefficients and Radii of Gap Electrodes Measured in Aqueous Solutions of Either 1 mM $K_3Fe(CN)_6$ or 1 mM $K_4Fe(CN)_6$ and Both 10 mM K_2HPO_4 and 0.1 M $NaClO_4$

	$Fe(CN)_6^{3-}$	$Fe(CN)_6^{4-}$
slope[a]	−5.5	+6.9
intercept	−20.0	−20.4
transfer coefficient, α	0.14	0.82
apparent radius[b] of the electrode (μm)	2.3−5.8	2.0−4.8

[a] We measured $E^{\circ\prime}$ to be 0.07 V (Ag wire) and 0.16 V (SCE) with bare gold. [b] The radii are calculated assuming standard rate constants of 1×10^{-2} to 6×10^{-2} cm/s.[15,17,18]

transfer of electrons from the redox-active species to the gold electrode.

The slopes of the plots in Figure 12 can be used to estimate values of α, the transfer coefficient (see Table 3). For films of gold covered with SAMs of $HO(CH_2)_nS$, the transfer coefficient of $Fe(CN)_6^{3-}$ was reported to decrease from 0.68 to 0.20 as n increased from 6 to 16.[20] The value of the transfer coefficient obtained from Figure 11 for $Fe(CN)_6^{3-}$ is not, therefore, characteristic of a "bare" gold surface. A plausible explanation of the small value of the transfer coefficient is the presence of organic material on the machined surfaces of the gap electrode. A likely origin of the organic material is remnants of the SAM that covered the surface of the gold prior to machining. We note, in addition, that low transfer coefficients have also been measured using small, gap-type electrodes and ferrocene in acetonitrile.[41]

Because the working electrode and counter electrode are separated by only 1 μm, the shapes of the cyclic voltammograms in Figure 11 can contain contributions due to the overlap of the concentration boundary layers that extend into solution from the surfaces of each electrode. To test the role of the overlap of boundary layers, the behavior of the gap electrodes was measured using only one of the electrodes in the gap (Figure 11b, broken line). An external platinum wire was used as the counter electrode. The cyclic voltammogram was unchanged from that measured using both electrodes in the gap.[45]

Conclusions

In this paper we report wet chemical methods to fabricate microstructures from gold. Cyclic voltammetry was used to demonstrate that these microstructures can function as microelectrodes. Three types of microstructures were prepared: grooves, wires, and gaps. Each of these microstructures had at least one dimension that was in the ~1-μm range or less. Because of their small dimensions, these electrodes showed electrochemical responses during cyclic voltammetry that reflected nonplanar diffusion of redox-active species in solution to the surface of the electrode.

The groove and supported wire electrodes produced cyclic voltammograms with little hysteresis and well-defined limiting currents; the measured limiting currents were consistent with estimates of the rate of mass transport of redox-active species to the electrode. Currents at "microgap" electrodes do not, however, appear to be limited by mass transport. Instead, the kinetics of electron transfer from the redox species to the gold appear to determine the voltammetric behavior of the electrodes.

(45) Note that the number of redox-active species that undergo electron transfer at the electrode during the course of the experiment is negligible compared to the number of those present within the 10–20-μL drop of solution. The measured cyclic voltammograms do not reflect, therefore, an exhaustion of the redox-active species within the drop.

Because groove and gap electrodes require the SAM to be electrically insulating, and because SAMs of $CH_3(CH_2)_{15}S$ do not insulate an underlying film of gold from a contacting solution of ferrocene in acetonitrile, these electrodes do not function with ferrocene in acetonitrile; the electrodes do, however, function in aqueous systems. The "microwire" electrodes, in contrast, can be used in both aqueous and nonaqueous solvents. The gap electrodes offer the potential to detect the presence of redox-active analytes in very small aqueous volumes of liquid (~1 fL).

The above voltammetric characteristics of these microelectrodes and the simplicity of the wet chemical method used to achieve their microfabrication offer an attractive approach for design, creation, and prototyping of micrometer-scale, electrically-conducting structures for electroanalytical and bioelectrochemical studies.

Experimental Section

Materials. Titanium (99.999+%), Au (99.999+%), ferrocene, $CH_3(CH_2)_{15}SH$, and $K_4Fe(CN)_6$ were obtained from Aldrich. $HO(CH_2)_2SH$ was obtained from Bio-Rad Laboratories. Acetonitrile and $K_3Fe(CN)_6$ were obtained from Mallinckrodt. $Ru(NH_3)_6Cl_3$ was obtained from Johnson Matthey. KOH and KCN were obtained from Fisher Scientific. All solvents and reagents were used as received. The water was deionized and distilled before use.

Preparation of Gold Films. Glass microscope slides (VWR Co.) were cleaned in piranha solution (30% H_2O_2 and 70% H_2SO_4) (**WARNING: Piranha solution should be handled with caution; in some circumstances (most probably when it has been mixed with significant quantities of an oxidizable organic material), it has detonated unexpectedly**), rinsed with distilled water, and dried in an oven prior to placement in the evaporation chamber. Titanium (~6 Å) was evaporated at 1 Å/s and gold (1000 Å) was evaporated at 5 Å/s onto clean glass microscope slides in a cryogenically-pumped chamber (base pressure $\sim 8 \times 10^{-8}$ Torr, operating pressure $\sim 1 \times 10^{-6}$ Torr) using an electron beam. This procedure results in the formation of gold films that are polycrystalline but have a predominant crystallographic orientation that is (111).[28]

Fabrication of Microstructures. A. "Microgroove" Electrodes. (i) SAMs were formed on the surfaces of the evaporated films of gold using the following procedure. First, the gold films were electrochemically conditioned by cycling the electrical potential of the film between −0.4 (SCE) and +1.4 V (SCE) in aqueous solutions of 0.1 M H_2SO_4 until the voltammograms were invariant between cycles (typically achieved within 10 cycles). Second, the electrochemically cleaned gold was washed in water and ethanol. Third, the films were placed in solutions of alkanethiol (1 mM in degassed ethanol or isooctane) for at least 24 h. (ii) A surgical scalpel (no. 11, Feather Industries) with a ~3-mN force (two paper clips) applied to its tip was used to micromachine an array of 1-μm-wide grooves into macroscopic gold films covered with SAMs of $CH_3(CH_2)_{15}S$. Grooves 8 μm wide were prepared by weighting the sample with a force of 30 mN (bulldog clip). The grooves were machined by suspending the scalpel between a pair of tweezers and moving the film of gold using a hand-operated $x-y$ micromanipulator stage.[8,9] (iii) The surface of the machined grooves was conditioned electrochemically by cycling the sample between −0.4 (SCE) and +1.4 V (SCE) in an aqueous solution of 0.1 M H_2SO_4.

B. Supported Microwires. (i) Macroscopic electrical contact pads were masked to contact by electrolyte by dipping both ends of the gold film sample (leaving a ~15-mm region of bare gold in the middle of the gold film) in neat hexadecanethiol for 20 s. (ii) The gold film was immersed in an ethanolic solution of $HO(CH_2)_2SH$ (~100 mM) for 10 min. (iii) The tip of a surgical scalpel was used to machine a micrometer-wide line of exposed gold into the surface of the gold film covered with $HO(CH_2)_2S$. (iv) A SAM was formed selectively on the micromachined regions of bare gold by immersing the sample in a concentrated (>10 mM) ethanolic solution of hexadecanethiol for 10 s. After immersion in the solution of hexadecanethiol, the sample was washed in heptane rather than ethanol. Washing in ethanol resulted in a

waxy residue on the surface of the gold and incomplete etching of the areas of the gold film covered with a monolayer of $HO(CH_2)_2S$. (v) Regions of the gold film covered with a monolayer formed from $HO(CH_2)_2SH$ were selectively etched by immersing the entire gold film in an aqueous solution of 1 M KOH and 0.1 M KCN that was sparged with O_2 and stirred vigorously. The time required to etch the sample to the glass substrate was typically ~45 min. (vi) The wire was inspected for defects using optical microscopy and checked to ensure that it was electrically conducting.

C. Microgap Electrode. The starting point for the preparation of microgap electrodes was a microwire (described above) connected between two macroscopic electrical contact pads. (i) The surface of the microwire was electrochemically cleaned by immersing the wire in an aqueous solution of 0.1 M H_2SO_4 and cycling the electrical potential between −0.4 and +1.4 V. (ii) The electrochemically cleaned microwire was immersed in an ethanolic solution containing ~10 mM $CH_3(CH_2)_{15}SH$ for at least 24 h. (iii) Cyclic voltammetry in 1 mM $K_3Fe(CN)_6$ (pH 7, 5 mM KH_2PO_4, 5 mM K_2HPO_4, 0.1 M $NaClO_4$) was used to confirm that an electrically insulating SAM of $CH_3(CH_2)_{15}S$ had formed on the surface of the microwire. (iv) A surgicial scalpel was used to micromachine a 1-μm-wide gap into the microwire. The resistance between the two electrical contact pads was measured to increase from approximately 2450 Ω before the gap was machined to in excess of 20 MΩ after machining of the gap. (v) The electrochemical behavior of the electrodes was measured by placing a 10−20-μL drop of the solution containing the redox-active species on the surface of the glass slide on which the electrodes were supported. A silver wire was inserted into the drop and was used as a reference electrode.

Cyclic Voltammetry. All solutions were deaerated by bubbling Ar prior to use. The reference electrode was either a saturated calomel electrode or a silver wire (diameter 0.1 mm). Before performing electrochemical measurements, the surface oxides were removed from the silver wire using an abrasive paper. Solutions were not stirred during measurement of the cyclic voltammograms. Measurements were performed using a signal generator (Princeton Applied Research Model 175 universal programmer) used in conjunction with a three-electrode potentiostat (Princeton Applied Research Model 174A polarographic analyzer).

Acknowledgment. Partial support of this research was provided by the Advanced Projects Research Agency and the Office of Naval Research. The authors thank Steven Bergens, Hans Biebuyck, and Watson Lees for useful suggestions and interesting discussions.